Eur. J. Mineral., 38, 669–677, 2026
https://doi.org/10.5194/ejm-38-669-2026
© Author(s) 2026. This work is distributed under
the Creative Commons Attribution 4.0 License.

European Journal of Mineralogy
Open Access

New insights into the high-pressure behaviour of the cyclosilicate benitoite, $BaTiSi_3O_9$

Benedetta Chrappan Soldavini[1], Davide Comboni[1], Gaston Garbarino[2], Michael Hanfland[2], and Marco Merlini

[1]Dipartimento di Scienze della Terra, Università degli Studi di Milano, Via Botticelli 23, 20133 Milano, Italy
[2]ESRF – European Synchrotron Radiation Facility, 71 Avenue des Martyrs, CS40220, 38043 Grenoble CEDEX, France

Correspondence: Davide Comboni (davide.comboni@unimi.it)

Received: 27 February 2026 – Revised: 6 July 2026 – Accepted: 27 August 2026 – Published: 6 November 2026

Abstract. The high-pressure behaviour of benitoite (ideally $BaTiSi_3O_9$, $a \sim 6.64$ Å, $c \sim 9.76$ Å, space group $P\bar{6}c2$) was studied at ambient temperature by single-crystal X-ray diffraction up to 22.3 GPa using a diamond anvil cell and He as a quasi-hydrostatic pressure-transmitting medium. High-pressure data revealed three phase transitions, occurring between 3.93(5)–4.40(5) GPa (from benitoite to benitoite-II), between 12.44(5)–13.05(5) GPa (from benitoite-II to benitoite-III), and between 16.36(5)–17.08(5) GPa (from benitoite-III to benitoite-IV). The P–V data were fitted with a second-order Birch–Murnaghan equation, allowing the determination of the elastic parameters for benitoite, benitoite-II, and benitoite-III. The benitoite-to-benitoite-II transition presents a second-order character, consistent with previous literature, whereas the transitions from benitoite-II to benitoite-III and from benitoite-III to benitoite-IV are accompanied by a volume discontinuity, more pronounced in the latter. The structures of benitoite-III (space group $Pbn2_1$) and benitoite-IV (space group $R32$) have been solved. A progressive deformation of the Si_3O_9 rings is observed, with the tilting angle of tetrahedral edges gradually increasing from benitoite to benitoite-II and to benitoite-III. In benitoite-IV the topology of one Si_3O_9 ring is significantly different from the lower-pressure polymorphs in that the basal faces of the three tetrahedra are almost parallel; these mechanisms are primarily correlated with the overall increase in density, along with the deformation of the TiO_6 octahedra and an overall increase in the Ba coordination number. Understanding the structural characteristics of benitoite and its behaviour under high-pressure conditions provides valuable insights into the stabilization mechanisms of the three-fold ring in various polymorphs, with broader implications for other chemical systems, such as the $CaSiO_3$ system. Additionally, the findings may offer meaningful insights into the behaviour of high-pressure polymorphs of carbonates with sp^3-hybridized carbon.

1 Introduction

Benitoite (ideally $BaTiSi_3O_9$, $a \sim 6.64$ Å, $c \sim 9.76$ Å, space group $P\bar{6}c2$) is an extremely rare mineral species, and its occurrence has been confirmed in just nine locations worldwide. Only the Benitoite Gem mine (California, USA) and four other mines nearby have produced gem-quality material (Wise and Gill, 1977). Here, benitoite was found in hydrothermally altered serpentine near the headwaters of the San Benito River (California, USA), from which it takes its name (Louderback and Blasdale, 1907). There is considerable controversy regarding the first discovery of this phase, and it seems that it was initially misinterpreted as sapphire (Louderback and Blasdale, 1909; Austin, 1988; Laurs et al., 1997) due to its appearance. The colour of benitoite crystals is quite variable and ranges from blue to violet blue (totally and pink benitoite samples are extremely rare), while the intensity varies from very light to medium dark. Strong dichroism, from colourless to blue, is evident to the eye and through a dichroscope (Gaft et al., 2004). Blue benitoite crystals mined in the Benito and Fresno counties are currently used as gemstones. The study of Louderback and Blasdale (1909)

contains plenty of details regarding the geological setting of the discovery site, and the authors also provided wet chemical analyses and described its physical and optical properties. Later, the chemical composition was re-investigated by Laird and Albee (1972) via electron microprobe analysis, whereas its structure was initially solved by Zachariassen (1930) and was later refined and essentially confirmed by Fisher (1969). In benitoite, groups of three SiO_4 tetrahedra are connected to form rings with $\bar{6}$ symmetry. The Ba and Ti atoms lie on three-fold symmetry axes parallel to the c crystallographic direction in two-fold positions ($2e$ and $2c$ respectively) on either side of a mirror plane. At ambient pressure, barium displays an unusual $[6+6]$-fold coordination, but if only the six shortest distances are considered (Ba–O $\sim$ 2.76 Å), Ba is in a distorted octahedral coordination.

Titanium is octahedrally coordinated to six oxygen atoms (Ti–O $\sim$ 1.95 Å) belonging to the unshared corners of the triangular $[Si_3O_9]^{6-}$ ring. Therefore, the crystal structure of benitoite (Fig. 1) can be viewed as a stacking of titanium silicate complexes (with $[Ti(Si_3O_9)_6]^{32-}$ stoichiometry) in which the Ba site fills the gaps (Henry, 1998; Gaft et al., 2004; Hejny et al., 2012). The high-pressure behaviour of benitoite has been previously studied by Hejny et al. (2012), who detected a second-order phase transition at approximately 4.2 GPa. Diffraction experiments indicate a second-order phase transition with $a' = a\sqrt{3}$ and $c' = c$ relative to the $P\bar{6}c2$ sub cell. The high-pressure phase of benitoite (hereafter referred to as benitoite-II) was resolved by Hejny et al. (2012) in the $P31c$ space group.

The symmetry breaking, as reported by the authors, leads to a splitting of the single Ba site into three sites occupying the Wyckoff positions $2a$ (0, 0, z) and $2b$ (1/3, 2/3, z; 2/3, 1/3, z). Moreover, the Ti site changes its special position, from $2c$ (point symmetry 32) in the ambient-pressure benitoite to $6c$ (point symmetry 1). The geometrical relationship and the structures of the two polymorphs are displayed in Fig. 1. Hejny et al. (2012) also reported that the structural changes induced by the phase transition have an effect on the bulk modulus (i.e. $K_{V0} = \beta^{-1}$, where β is the compressibility parameter), decreasing its bulk modulus from $K_0 = 117.9(7)$ GPa for benitoite to $K_0 = 88.9(1.6)$ GPa for benitoite-II. However, because of the relatively low hydrostatic limit of the used pressure medium (water-free 4 : 1 methanol–ethanol mixture), the authors decided to conclude the experiment at 6.14 GPa in order to avoid shear stresses which could decrease the quality of the diffraction peaks (Angel et al., 2007; Klotz et al., 2009). Nevertheless, benitoite is rather interesting due to the presence of the $(Si_3O_9)^{6-}$ silicate-ring units, which is a relatively uncommon feature in silicates. Only $CaSiO_3$ pseudowollastonite present a structure with three-fold silicate ring units with the same topology as benitoite (Yang and Prewitt, 1999). However, it is known that wollastonite or pseudowollastonite transform with pressure and temperature into new high-pressure polymorphs, namely breyite and parabreyite, featuring three-fold silicate rings but with different topologies (Brenker et al., 2021; Chrappan Soldavini et al., 2025). Considering the interest of the $CaSiO_3$ system for the Earth's inner mineralogy, a high-pressure study on benitoite is a rather relevant comparative system to be investigated. Moreover, recent high-pressure research on carbonates, for instance, Fe-bearing $MgCa(CO_3)_2$ and Fe-bearing $MgCO_3$, has revealed that, at pressures above 80 GPa, both the compounds transform into new structures based on rigid three-fold tetrahedral carbonate rings (Merlini et al., 2017; Chariton et al., 2020). Due to limited possibilities to systematically investigate the crystal chemistry of candidate high-pressure carbonate minerals, studies conducted on silicates with similar structural features do allow comparative studies relevant to identifying possible different polymorphs in the same way studies on germanates drove the pioneering crystal chemistry of high-pressure silicates a few decades ago (e.g. Ringwood and Major, 1967).

Here, we report the results of a high-pressure X-ray experiment on single crystal of benitoite using a diamond anvil cell and He as the pressure-transmitting medium up to 22.36(5) GPa (numbers in parentheses are the standard uncertainties (s.u.) of the last significant digits according to IUCr guidelines). The main aim of this study is to extend the pressure range of the experiments reported by Hejny et al. (2012), providing new insights into the high-pressure behaviour and polymorphism of benitoite. We observed three distinct high-pressure phase transitions, two of which have not been reported previously.

2 Experimental procedures

A sample of benitoite from San Benito River (California, USA), provided by the Earth Sciences Museum Ardito Desio (Milan), was used in this study. A small single crystal fragment of about $20 \times 10 \times 10$ µm was loaded into a membrane-driven diamond anvil cell (DAC), with 600 µm culet Boehler–Almax design anvils, along with a ruby sphere for pressure determination (pressure uncertainty ± 0.05 GPa, Mao et al., 1986). A stainless-steel foil (with an initial thickness $of \sim 250$ µm) was pre-indented to 90 µm and then drilled by spark erosion, leading to a P chamber of $\sim$ 300 µm in diameter; He was used as the pressure medium. An in situ high-pressure single-crystal synchrotron X-ray diffraction experiment was performed at the ID15b beamline, ESRF, Grenoble (France). A convergent monochromatic beam ($E \sim 30$ keV, $\lambda = 0.41069$ Å, spot size $\sim 5 \times 6$ µm) was used for the diffraction experiment. Diffraction images were acquired with a Mar555 flat-panel detector, using an in-house script for collecting step scan diffraction images. Sample-to-detector distance ($\sim$ 260 mm) was calibrated using an Si standard and an enstatite ($MgSiO_3$) crystal. Further details on the beamline setup are reported in Merlini and Hanfland (2013). Load was applied to the diamond anvil cell with an automated gas-membrane-driven system, and pres-

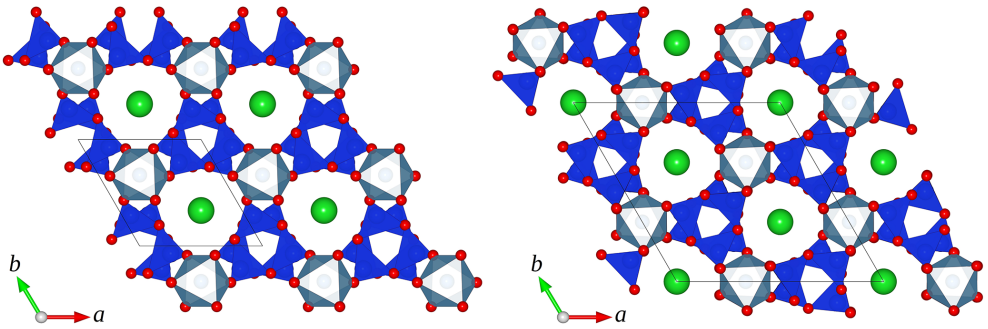


Figure 1. Schematic representations of unit cell of benitoite and the high-pressure polymorph, benitoite-II, solved by Hejny et al. (2012). SiO_4 tetrahedra in blue, TiO_6 octahedra in light blue, Ba cations in green.

sure in the sample chamber was determined with the online ruby–alignment system after an average equilibration time of 15 min. The adopted data collection strategy consisted of a simple ω scan ($-32° \leq \omega \leq +32°$), with 0.5° step width and 0.25 s exposure time per step. The diffraction images were then converted into the "Esperanto" format in order to be analysed with the software CrysAlis (Rothkirch et al., 2013; Rigaku Oxford Diffraction, 2018). Indexing of the diffraction peaks and integration of their intensities (corrected for Lorentz-polarization effects) were performed using the CrysAlis package (Rigaku Oxford Diffraction, 2018). Corrections for absorption (caused by the DAC components) were applied using the semi-empirical ABSPACK routine implemented in CrysAlis (Rigaku Oxford Diffraction, 2018). All the structure refinements were performed using the package JANA2006 (Petříček et al., 2014). To assess the reversibility of the detected phase transitions and investigate their hysteresis, a few measures were taken in decompression. Selected reconstructions of reciprocal lattice planes in the four polymorphs are shown in Fig. S1 in the Supplement. The unit-cell parameters at high pressure are listed in Table 1, and the evolution with pressure of the volume per formula unit is shown in Fig. 2.

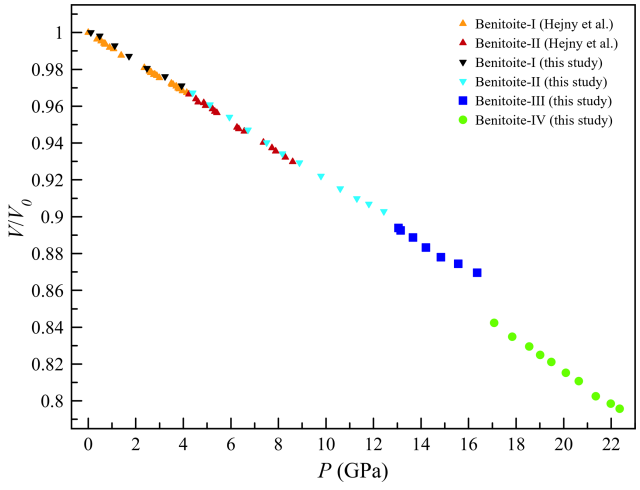


Figure 2. Evolution of the normalized unit-cell volume (V_0) of benitoite. Data collected by Hejny et al. (2012) in upward triangles (orange and red for benitoite and benitoite-II, respectively). Data collected in this experiment in downward triangles (black and sky blue for benitoite and benitoite-II, respectively; benitoite-III in blue squares and benitoite-IV in green circles).

3 Refinement protocols

For benitoite and benitoite-II, the structures reported by Hejny et al. (2012) were used as starting models, refining the displacement parameters of all atoms as isotropic (Table S1 in the Supplement); no restraint on bond distances or angles was used. Two phase transitions were observed between 12.44(5) and 13.05(5) GPa and between 16.36(5) and 17.08(5) GPa, respectively. The newly discovered polymorphs will be referred to as benitoite-III and benitoite-IV. The structures of benitoite-III and benitoite-IV were solved using the *Superflip* software (Palatinus and Chapuis, 2007), implemented in JANA2006, to locate most of the crystallographic sites. A careful analysis of the difference–Fourier electron density maps allowed for the location of the remaining missing atoms; crystallographic information files (CIFs) are submitted as part of the Supplement. The structural changes associated with the individual phase transitions will be discussed in the next sections. The principal statistical parameters of the structure refinements are listed in Table S1, and inter-atomic angles and relevant distances, calculated by the Diamond and Vesta software (Momma and Izumi, 2008), are reported in Tables S2, S3, and S4.

4 Results

4.1 Elasticity of benitoite

In order to describe the compressional behaviour of the benitoite polymorphs, the coefficients of the Birch–Murnaghan equation of state (BM-EoS) were fitted to the experimental P–V data (Birch, 1947) using the EoSFitGUI software (Angel et al., 2014). The f_e–F_e plot (where $f_e = [(V_0/V)^{2/3} -$

Table 1. Unit-cell parameters of the different polymorphs of benitoite with pressure (* data collected in decompression).

P (GPa)	Polymorph	Sp. Gr.	V (Å^3)	a (Å)	c (Å)	b (Å)	Dataset
0.11(5)	benitoite	$P\bar{6}c2$	372.30(2)	6.637(2)	9.7581(3)		1
0.49(5)	benitoite	$P\bar{6}c2$	371.61(7)	6.6333(6)	9.752(1)		2
1.12(5)	benitoite	$P\bar{6}c2$	369.64(3)	6.6196(2)	9.7404(5)		3
1.71(5)	benitoite	$P\bar{6}c2$	367.51(2)	6.6061(2)	9.7240(3)		4
2.47(5)	benitoite	$P\bar{6}c2$	365.07(2)	6.5903(2)	9.7061(3)		5
3.23(5)	benitoite	$P\bar{6}c2$	363.40(2)	6.5788(2)	9.6951(4)		6
3.93(5)	benitoite	$P\bar{6}c2$	361.54(2)	6.5667(2)	9.6812(3)		7
4.40(5)	benitoite-II	$P31c$	1080.3(1)	11.3582(5)	9.6693(6)		8
5.12(5)	benitoite-II	$P31c$	1073.12(5)	11.3342(3)	9.6457(3)		9
5.94(5)	benitoite-II	$P31c$	1065.59(4)	11.3090(2)	9.6208(3)		10
6.72(5)	benitoite-II	$P31c$	1057.83(4)	11.2833(2)	9.5944(2)		11
7.51(5)	benitoite-II	$P31c$	1050.12(6)	11.2576(3)	9.5679(4)		12
8.17(5)	benitoite-II	$P31c$	1043.41(6)	11.2351(3)	9.5448(4)		13
8.89(5)	benitoite-II	$P31c$	1037.95(8)	11.2172(5)	9.5252(5)		14
9.79(5)	benitoite-II	$P31c$	1029.85(8)	11.1903(4)	9.4965(5)		15
10.60(5)	benitoite-II	$P31c$	1022.22(9)	11.1647(5)	9.4694(6)		16
11.30(5)	benitoite-II	$P31c$	1016.22(7)	11.1447(4)	9.4475(5)		17
11.81(5)	benitoite-II	$P31c$	1012.89(6)	11.1340(4)	9.4348(4)		18
12.44(5)	benitoite-II	$P31c$	1008.38(1)	11.1191(4)	9.4179(4)		19
13.05(5)	benitoite-III	$Pbn2_1$	665.6(2)	6.4863(2)	10.9523(9)	9.369(1)	20
13.14(5)	benitoite-III	$Pbn2_1$	664.6(2)	6.4867(2)	10.948(1)	9.359(1)	20-2
13.66(5)	benitoite-III	$Pbn2_1$	661.74(6)	6.4874(6)	10.920(1)	9.341(1)	21
14.21(5)	benitoite-III	$Pbn2_1$	657.68(7)	6.4814(3)	10.8896(7)	9.3183(6)	22
14.84(5)	benitoite-III	$Pbn2_1$	653.77(9)	6.4764(4)	10.8593(9)	9.2929(8)	23
15.57(5)	benitoite-III	$Pbn2_1$	651.12(1)	6.474(1)	10.8395(4)	9.2781(8)	24
16.36(5)	benitoite-III	$Pbn2_1$	647.50(8)	6.4719(7)	10.8089(3)	9.2562(6)	25
17.08(5)	benitoite-IV	$R32$	2814.7(1)	10.8250(2)	27.8132(9)		26
17.84(5)	benitoite-IV	$R32$	2797.3(1)	10.7706(3)	27.8443(8)		27
18.55(5)	benitoite-IV	$R32$	2779.6(1)	10.7294(2)	27.8801(8)		28
19.01(5)	benitoite-IV	$R32$	2764.24(9)	10.6935(2)	27.9127(6)		29
19.48(5)	benitoite-IV	$R32$	2751.4(1)	10.6634(2)	27.9404(7)		30
20.09(5)	benitoite-IV	$R32$	2731.7(2)	10.6113(3)	28.014(1)		31
20.63(5)	benitoite-IV	$R32$	2716.6(2)	10.5675(3)	28.090(1)		32
21.35(5)	benitoite-IV	$R32$	2689.1(2)	10.4975(4)	28.177(1)		33
21.98(5)	benitoite-IV	$R32$	2675.6(2)	10.4601(3)	28.237(1)		34
22.36(5)	benitoite-IV	$R32$	2666.4(2)	10.4345(3)	28.278(1)		35
5.70*(5)	benitoite-II	$P31c$	1067.44(9)	11.3114(5)	9.6335(5)		36
3.59*(5)	benitoite	$P\bar{6}c2$	362.10(5)	6.5707(4)	9.6844(9)		37
1.34*(5)	benitoite	$P\bar{6}c2$	368.93(4)	6.6152(3)	9.7349(6)		38
0.66*(5)	benitoite	$P\bar{6}c2$	370.97(2)	6.6283(2)	9.7501(3)		39
0.01*(5)	benitoite	$P\bar{6}c2$	373.10(2)	6.6423(2)	9.7648(3)		40

1]/2 is the Eulerian finite strain and F_e is the normalized pressure, defined as $F_e = P/3\ f_e\ (1+2f_e)^{5/2}$; Birch, 1947; Angel et al., 2014), for benitoite polymorphs led to the conclusion that the truncation to the second-order of the BM-EoS provides the best figure of merit (Fig. S2). The Birch–Murnaghan equation of state (EoS) allows us to refine the bulk modulus (K_{V0} or $K_{P0,T0}$, defined as $-V_0(\partial P/\partial V)_{T0} = \beta^{-1}_{P0,T0}$, where $[\beta_{P0,T0}]$ is the volume compressibility coefficient at room conditions) and its P derivatives ($K' = \partial K_{P0,T0}/\partial P$ and $K'' = \partial^2 K_{P0,T0}/\partial P^2$). Truncated to the second order in energy, i.e. with $K' = \partial K_{P0,T0}/\partial P = 4$, the EoS transforms into $P\ (f_e) = 3K_{P0,T0}\ f_e\ (1+2f_e)^{5/2}$.

Accordingly, the benitoite data were fitted using a second-order BM-EoS with K' fixed at 4, yielding $K_{V0} = 118(3)$ GPa and $\chi^2_w = 3.25$. Benitoite-II data were also fitted with a second-order BM-EoS, which resulted in $V_0 = 1131(3)$ Å^3, $K_0 = 90(6)$ GPa ($\chi^2_w = 1.37$). The obtained BM-EoS parameters are listed in Table 2. It should be noted that the pressure stability fields of benitoite-II, benitoite-III, and benitoite-IV are relatively narrow. Consequently, the corresponding EoS fits are based on a limited finite-strain in-

Table 2. Refined elastic parameters (e.g. K_{V0}, the bulk modulus, and its derivate K') pertaining to the different polymorphs of benitoite based on the isothermal II-BM equation of state fits (* fixed parameter).

Benitoite	V_0, x_0 (Å^3, Å)	K_{V0}, M_{x0} (GPa)	K'	$\beta_{V0,x0}$ (GPa^{-1})
V	372.9(2)	118(3)	4*	0.0085(2)
a	6.642(1)	318(9)	4*	0.00314(9)
c	9.761(1)	446(14)	4*	0.00224(7)
II-BM EoS, $P < 3.93(5)$ GPa				
Benitoite-II	V_0, x_0 (Å^3, Å)	K_{V0}, M_{x0} (GPa)	K'	$\beta_{V0,x0}$ (GPa^{-1})
V	1134.2(9)	83.2(9)	4*	0.0120(1)
a	11.526(3)	277(3)	4*	0.00361(4)
c	9.861(9)	205(6)	4*	0.0049(1)
II-BM EoS, 4.40(5) GPa $< P <$ 12.34(5) GPa				
Benitoite-III	V_0, x_0 (Å^3, Å)	K_{V0}, M_{x0} (GPa)	K'	$\beta_{V0,x0}$ (GPa^{-1})
V	772(8)	65(5)	4*	0.0154(2)
a	6.56(1)	1060(141)	4*	0.0009(1)
b	10.06(6)	117(13)	4*	0.0085(9)
c	11.91(7)	93(9)	4*	0.011(1)
II-BM EoS, 13.05(5) GPa $< P <$ 16.36(5) GPa				

terval, which reduces the ability to independently constrain V_0 and K_0. As a result, these parameters are strongly correlated, and their uncertainties are likely to be larger than those suggested by the formal least-squares standard deviations. The Birch–Murnaghan fit was performed considering an estimated uncertainty of ±0.05 GPa for pressure (Mao et al., 1986). As reported in Fig. 2, the volume evolutions with pressure for benitoite and benitoite-II show no significant variation. Indeed, the bulk moduli of benitoite and benitoite-II are not distinguishable within 3σ, and the obtained parameters are consistent within 1σ with the values obtained by Hejny et al. (2012). For benitoite-III, only seven data points were collected over a limited pressure interval (∼ 13.05(5)–16.36(5) GPa), resulting in a poorly constrained EoS fit. Consequently, the refined values of V_0 and K_0 are strongly correlated and should be regarded as indicative rather than uniquely determined.

Fitting the data with a second-order BM-EoS resulted in $V_0 = 772(8)$ Å^3 and $K_0 = 65(5)$ GPa with $\chi^2_w = 6.26$. Attempts to use a higher-order BM-EoS did not converge during the least-squares fitting process.

Benitoite showed an interesting behaviour upon compression since the c unit cell parameter increases with pressure (27.7862(9) Å at 17.08(5) GPa and 28.278(1) Å at 22.36(5) GPa). Few measurements were taken in decompression, and no residual deformation was observed under room-pressure conditions (Table 1).

4.2 Structural deformation mechanisms in the observed phase transitions

The benitoite-to-benitoite-II phase transition has been already observed and discussed in detail by Hejny et al. (2012). The symmetry breaking from $P\bar{6}c2$ to $P31c$ leads to a splitting of the single Ba site into three sites (Ba1, Ba2, Ba3), whereas the Ti site remains unique. Moreover, the Si and O atoms in benitoite-II also split their positions into three different sites. Additionally, the z coordinates of Si and O1, which are located in special positions in benitoite, become general positions in benitoite-II. In order to address some comparisons between the other high-pressure polymorphs, we have maintained the same straightforward naming scheme proposed by Hejny et al. (2012), who named the split oxygen atoms as O11, O12, O13, O21, O22, O23, O21m, O22m, and O23m and the Si atoms as Si1, Si2, and Si3. In benitoite-II the octahedral coordination of the Ti atoms is, immediately after the transition, regular, with only small differences between the individual Ti–O bond distances (ranging between 1.908(9) and 1.95(1) Å at 4.40(5) GPa); however, at 12.44(5) GPa, the Ti–O bond distances range between 1.97(1) and 1.81(1) Å. Between 12.44(5) and 13.05(5) GPa benitoite-II undergoes a second phase transition, characterized by a further decrease in the crystal symmetry (from $P31c$ to $Pbn2_1$), and, remarkably, the c unit-cell lattice of benitoite-II is parallel to the b unit-cell lattice of benitoite-III, as can be seen in Fig. 3. Figure S1 shows the reconstruction of relevant crystallographic planes, and, in *h0l*, it is possible to discern groups of three deformed diffraction spots, very close to one another.

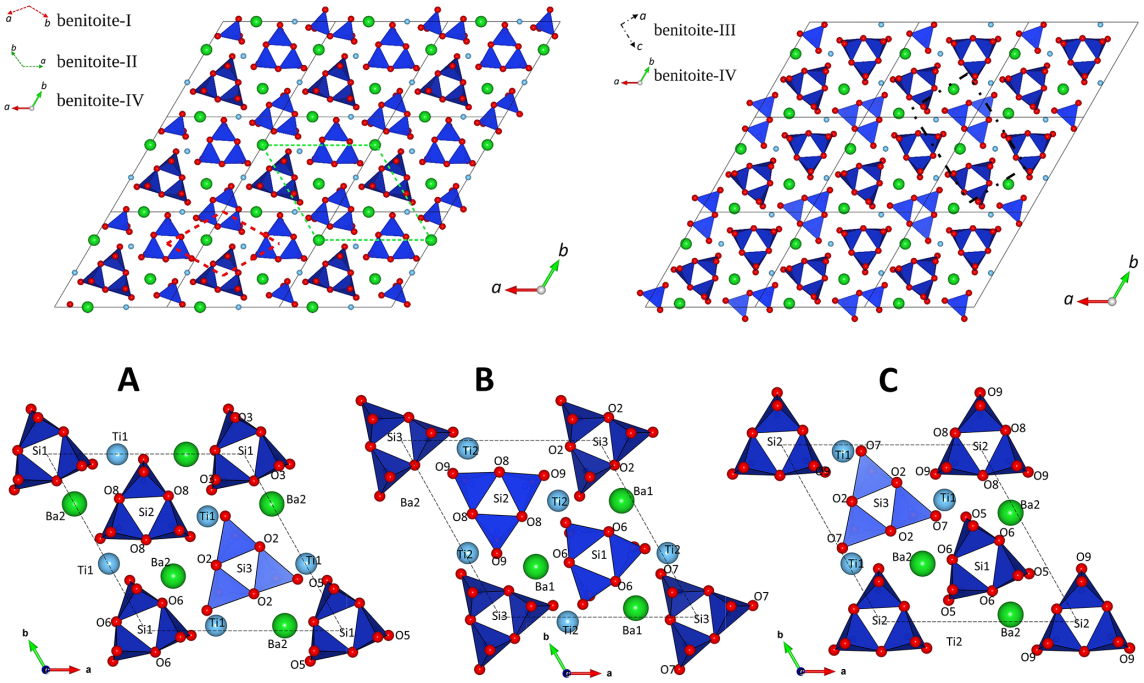


Figure 3. Schematic representations of the unit cells of benitoite-IV viewed along the *c* axis, highlighting key geometric relationships between the other polymorphs.

The elongated shapes of the reflections seem to suggest a rotation of the orthorhombic lattice on [010], and the presence of groups of three diffraction peaks on the *h0l* plane (Fig. S1) may suggest a pseudo-hexagonal twin lattice, consisting of three orthorhombic cells. Notably, this second phase transition also starts to affect the Ti–O_6 octahedra.

Polyhedra volumes, average bond distances, and bond angle variances were calculated by VESTA software (Momma and Izumi, 2008). The Ti–O distances in benitoite-II become rather uneven at high pressure, and, immediately before the benitoite-II-to-benitoite-III phase transition, the difference between the shortest and the longest Ti–O distance is about 0.16(2) Å (Table S2). The deformation of the Ti–O_6 octahedra continues in the $Pbn2_1$ polymorph (benitoite-III). The Ti–O average distance decreases, but the gap between the shortest and the longest distances remains quite high (0.12(3) Å at 13.05(5) GPa, Table. S2). In benitoite-III, the Ba cations display a nine-fold coordination. Due to the decrease in the crystal symmetry, all nine oxygen sites coordinated with the Ba cation occupy a unique position; overall, distances decrease modestly (Table S3) with pressure, and no major change regarding the Ba-polyhedra is observed.

4.3 Benitoite-III-to-benitoite-IV phase transition

Between 16.36(5) and 17.08(5) GPa, benitoite undergoes a third phase transition, from $Pbn2_1$ to $R32$. Unlike the previous phase transitions, which did not lead to major changes from a structural point of view, the benitoite-III-to-benitoite-

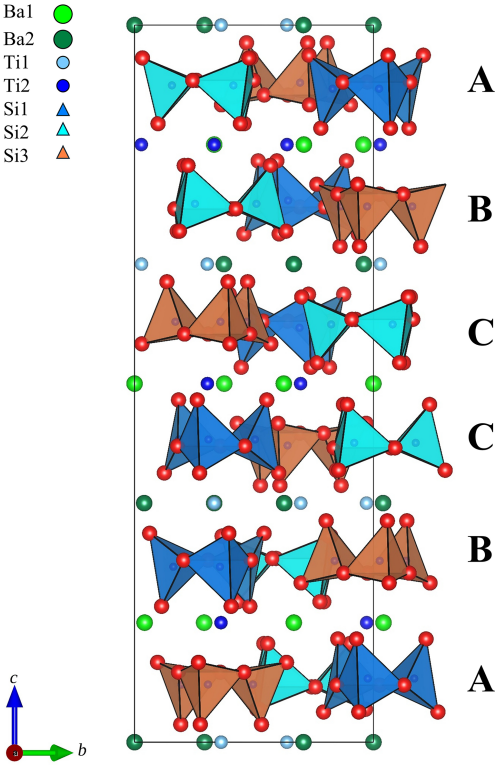


Figure 4. View parallel to the *a* crystallographic axis of benitoite-IV.

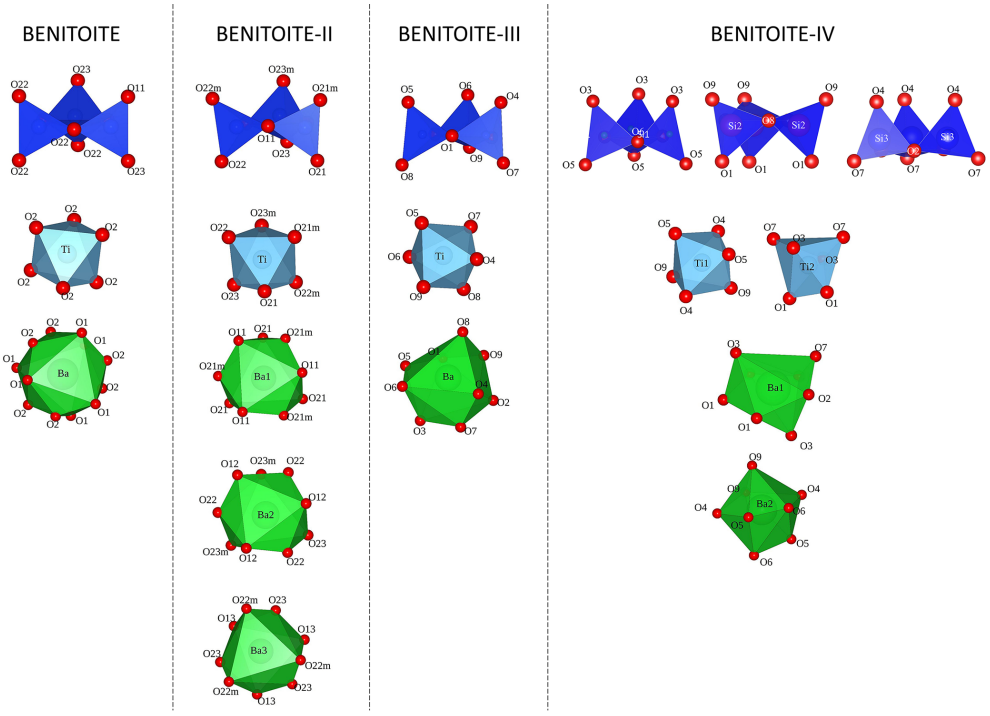


Figure 5. Reconstruction of the different polyhedral units in all benitoite polymorphs.

IV phase transition is characterized by several relevant deformation mechanisms. First, the structure seems to consist of the stacking, along the [001] crystallographic direction, of three different layers (hereafter referred to as A, B, and C) of Si tetrahedra, separated by the Ba and Ti cations, stacked following an ABCCBA order (Figs. 3 and 4). The main difference between the three layers is the different positions of the Si1, Si2 and Si3 tetrahedra (Fig. 3). Moreover, in the benitoite and benitoite-II polymorphs, the Ba and Ti sites occupy just one crystallographic site, but, in benitoite-IV, these cations split into two independent sites, named Ba1 and Ba2 and Ti1 and Ti2. As can be seen in Fig. 4, the stacking along the [001] direction also concerns these cations: the pair Ba1–Ti2 separates the A–B and C–C layers, whereas the pair Ba2–Ti1 divides the C–B and A–A layers. Another main difference between benitoite-IV and the other benitoite polymorphs is the deformation of the three-membered rings. At ambient pressure, in benitoite, the rings are perfectly symmetric, displaying $\bar{6}$ symmetry, with Si and O1 being located on the mirror plane, and the three-membered rings are arranged in layers perpendicular to the [001] crystallographic direction. Immediately after the benitoite-to-benitoite-II phase transition, at 4.40 (5) GPa, the three-membered rings break the $\bar{6}$ symmetry. The rings initially appear to be only slightly deformed, but their distortion increases with pressure. In benitoite-III, the deformation of the three-membered rings increases even more, further deviating from the original $\bar{6}$ symmetry.

Finally, in benitoite-IV, the deformation of the tetrahedral ring results in a different configuration, with two of the three rings having almost parallel tetrahedral basal faces. This structural modification also results in a density increase, from 4.241 to 4.379 g cm^3 ($\approx 3.2\,\%$) (see also Fig. S3). Looking at the unit-cell parameters, reported in Table 1, it is interesting to note that the c unit-cell edge increases with pressure in benitoite-IV. This is due to the tilting, around the oxygen hinges, of the Si and Ti coordination tetrahedra. This tilting leads to a progressive opening of the T1–Si_n–Ti2 intercationic angles ($n = 1$, 2, 3; Table S4) since such tilting is positively correlated with the progressive deformation of the Ti polyhedra (Table S3), leading to the conclusion that this can be the driving deformation mechanism of the steady increase in the c unit-cell edge.

4.4 Implications for the $CaSiO_3$ system

As aforementioned, benitoite represents a topological analogue of pseudowollastonite, the high-temperature polymorph of wollastonite: both structures are characterized by three-fold ring silicon tetrahedra with quasi-parallel external edges (i.e. edges between O22–O22, O23–O22, and O11–O23 in benitoite structure, Fig. 5). In this study, we report the structural determination of benitoite-IV, which, indeed, has the same topology as another high-pressure and high-temperature polymorph of wollastonite, initially identified as Ca-walstromite and later renamed breyite following its discovery in natural rocks (Joswig et al., 1999; Anzolini et al.,

2016; Woodland et al., 2020; Brenker et al., 2021). The two structures are characterized by three-fold ring tetrahedra with apical oxygens (i.e. O4 or O5 in benitoite-IV, depending on which tetrahedra is considered, Fig. 5) pointing in the same direction. The $CaSiO_3$ phase diagram available in the literature shows no direct relation between these two three-fold ring structures, with an intermediate field in which chain-structured wollastonite should still be stable (Chatterjee et al., 1984; Belmonte et al., 2017).

This is further supported by the quenchable nature of breyite, which can remain metastable at room pressure and temperature after synthesis. In this study, we found that such structural reorganization under pressure can be reached via two intermediate states: benitoite-II and benitoite-III, showing that the two structures can indeed be related by simple distortion and/or dislocation mechanisms. Although only limited compressibility studies have been conducted on pseudowollastonite, available literature data indicate no phase transitions up to 10.64(5) GPa (Yang and Prewitt, 1999; Chrappan Soldavini et al., 2025). Our results highlight the need for additional compressibility studies to explore any potential phase boundary between pseudowollastonite and breyite, which would have significant implications for the high-temperature region of the $CaSiO_3$ phase diagram.

5 Conclusions

The high-pressure evolution of benitoite structure reveals the existence of four polymorphs in the pressure interval of 0–20 GPa, characterized by a progressive distortion of the three-fold tetrahedral silicate ring and Ba and Ti polyhedra. Benitoite, $BaTiSi_3O_9$-II, and $BaTiSi_3O_9$-III present similar topology of the tetrahedral units, while $BaTiSi_3O_9$-IV presents a different configuration of two out of three silicate rings, with a tetrahedral base that is almost parallel. This resulted in a significant overall density increase. A similar behaviour is observed in the $CaSiO_3$ system, where breyite and parabreyite, which feature distorted three-membered rings, are significantly denser compared to pseudo-wollastonite. Both benitoite and $CaSiO_3$ provide valuable examples to explore the mechanism governing three-fold ring deformation under pressure and consequent structural variation. Other relevant examples of three-fold tetrahedral ring-based structures are constituted by high-pressure carbonates. Although only a few high-pressure polymorphs have been experimentally resolved for these carbonates with sp^3-hybridized carbon (e.g. $MgCO_3$-II, dolomite-IV, and predicted $CaCO_3$ phases), the complexity observed in benitoite suggests that similar structural variability could exist in carbonate systems. These may include multiple carbonate polymorphs and extensive solid solutions stabilized under lower mantle conditions, highlighting the potential richness under lower mantle conditions.

Data availability. Data will be made available upon request.

Supplement. The supplement related to this article is available online at https://doi.org/10.5194/ejm-38-669-2026-supplement.

Author contributions. BCS: data curation, validation, writing (review and editing). DC: data curation, formal analysis, writing (original draft, review and editing). GG: investigation. MH: investigation. MM: conceptualization, validation, writing (review and editing).

Competing interests. The contact author has declared that none of the authors has any competing interests.

Disclaimer. Publisher's note: Copernicus Publications remains neutral with regard to jurisdictional claims made in the text, published maps, institutional affiliations, or any other geographical representation in this paper. The authors bear the ultimate responsibility for providing appropriate place names. Views expressed in the text are those of the authors and do not necessarily reflect the views of the publisher.

Acknowledgements. ESRF is thanked for the allocation of the beam time (in-house proposal IH-ES-44, ref. no 89120).

Review statement. This paper was edited by Paola Comodi and reviewed by two anonymous referees.

References

Angel, R. J., Bujak, M., Zhao, J., Gatta, G. D., and Jacobsen, S. D.: Effective hydrostatic limits of pressure media for high-pressure crystallographic studies, J. Appl. Crystallogr., 40, 26–32, https://doi.org/10.1107/S0021889806045523, 2007.

Angel, R. J., Gonzalez-Platas, J., and Alvaro, M.: EosFit7c and a Fortran module (library) for equation of state calculations, Z. Kristallogr., 229, 405–419, https://doi.org/10.1515/zkri-2013-1711, 2014.

Anzolini, C., Angel, R. J., Merlini, M., Derzsi, M., Tokár, K., Milani, S., Krebs, M. Y., Brenker, F. E., Nestola, F., and Harris, J. W.: Depth of formation of CaSiO3-walstromite included in super-deep diamonds, Lithos, 265, 138–147, https://doi.org/10.1016/j.lithos.2016.09.023, 2016.

Austin, D.: The Benitoite Story, Independently published, 80 pp., https://g30010.eos-intl.net/G30010/OPAC/Details/Record (last access date: 14 September 2026), 1988.

Belmonte, D., Ottonello, G., and Zuccolini, M. V.: Ab initio-assisted assessment of the CaO-SiO2 system under pressure, Calphad, 59, 12–30, https://doi.org/10.1016/j.calphad.2017.07.005, 2017.

Birch, F.: Finite elastic strain of cubic crystals, Phys. Rev., 71, 809–824, https://doi.org/10.1103/PhysRev.71.809, 1947.

Brenker, F. E., Nestola, F., Brenker, L., Peruzzo, L., and Harris, J. W.: Origin, properties, and structure of breyite: The second most abundant mineral inclusion in super-deep diamonds, Am. Mineral., 106, 38–43, https://doi.org/10.2138/am-2020-7513, 2021.

Chatterjee, N. D., Johannes, W., and Leistner, H.: The system CaO-Al2O3-SiO2-H2O: new phase equilibria data, some calculated phase relations, and their petrological applications, Contrib. Mineral. Petrol., 88, 1–13, https://doi.org/10.1007/BF00371406, 1984.

Chrappan Soldavini, B., Merlini, M., Gemmi, M., Parlanti, P., Fumagalli, P., Milani, S., and Poli, S.: Crystal structure and elastic properties of parabreyite: a new high-pressure ring silicate in the $CaSiO_3$ system, Eur. J. Mineral., 37, 13–24, https://doi.org/10.5194/ejm-37-13-2025, 2025.

Chariton, S., Bykov, M., Bykova, E., and Koemets, E.: The crystal structures of Fe-bearing MgCO3 sp2- and sp3-carbonates at 98 GPa from single-crystal X-ray diffraction using synchrotron radiation, Res. Commun., 3, 715–719, 2020.

Fisher, K.: Verfeinerung der Kristallstruktur von Benitoit $BaTi[Si_3O_9]$, Z. Kristallogr., 129, 222–243, https://doi.org/10.1524/zkri.1969.129.1-4.222, 1969.

Gaft, M., Nagli, L., Waychunas, G., and Weiss, D.: The nature of blue luminescence from natural benitoite $BaTiSi_3O_9$, Phys. Chem. Miner., 31, 365–373, https://doi.org/10.1007/s00269-004-0407-x, 2004.

Hejny, C., Miletich, R., Jasser, A., Schouwink, P., Crichton, W., and Kahlenberg, V.: Second-order P6c2–P31c transition and structural crystallography of the cyclosilicate benitoite, $BaTiSi_3O_9$, at high pressure, Am. Mineral., 97, 1749–1763, https://doi.org/10.2138/am.2012.4175, 2012.

Henry, M.: Retrosynthesis in inorganic crystal structures: Application to nesosilicate and inosilicate networks, Coord. Chem. Rev., 178–180, 1109–1163, https://doi.org/10.1016/S0010-8545(98)00167-2, 1998.

Joswig, W., Stachel, T., Harris, J. W., Baur, W. H., and Brey, G. P.: New Ca-silicate inclusions in diamonds – tracers from the lower mantle, Earth Planet. Sci. Lett., 173, 1–6, https://doi.org/10.1016/S0012-821X(99)00216-2, 1999.

Klotz, S., Chervin, J. C., Munsch, P., and Le Marchand, G.: Hydrostatic limits of 11 pressure transmitting media, J. Phys. D: Appl. Phys., 42, 075413, https://doi.org/10.1088/0022-3727/42/7/075413, 2009.

Laird, J. and Albee, A. L.: Chemical composition and physical, optical, and structural properties of benitoite, neptunite, and joaquinite, Am. Mineral., 57, 85–102, 1972.

Laurs, B. M., Rohtert, W. R., and Gray, M.: Benitoite from the New Idria district, San Benito County, California, Gems Gemol., 33, 166–187, 1997.

Louderback, G. D. and Blasdale, W. C.: Benitoite, a new California gem mineral, with chemical analysis, Univ. Calif. Dept. Geol. Sci. Bull., 5, 149–153, 1907.

Louderback, G. D. and Blasdale, W. C.: Benitoite, its paragenesis and mode of occurrence, Univ. Calif. Dept. Geol. Sci. Bull., 5, 331–380, 1909.

Mao, H. K., Xu, J., and Bell, P. M.: Calibration of the ruby pressure gauge to 800 kbar under quasi-hydrostatic conditions, J. Geophys. Res., 91, 4673–4676, https://doi.org/10.1029/JB091iB05p04673, 1986.

Merlini, M. and Hanfland, M.: Single-crystal diffraction at megabar conditions by synchrotron radiation, High Press. Res., 33, 511–522, https://doi.org/10.1080/08957959.2013.831088, 2013.

Merlini, M., Cerantola, V., Gatta, G. D., Gemmi, M., Hanfland, M., and Kupenko, I.: Dolomite-IV: Candidate structure for a carbonate in the Earth's lower mantle, Am. Mineral., 102, 1763–1766, https://doi.org/10.2138/am-2017-6101, 2017.

Momma, K. and Izumi, F.: VESTA: A three-dimensional visualization system for electronic and structural analysis, J. Appl. Crystallogr., 41, 653–658, https://doi.org/10.1107/S0021889808012016, 2008.

Palatinus, L. and Chapuis, G.: SUPERFLIP: A computer program for the solution of crystal structures by charge flipping in arbitrary dimensions, J. Appl. Crystallogr., 40, 786–790, https://doi.org/10.1107/S0021889807029238, 2007.

Petříček, V., Dušek, M., and Palatinus, L.: Crystallographic computing system JANA2006: General features, Z. Kristallogr., 229, 345–352, https://doi.org/10.1515/zkri-2014-1737, 2014.

Ringwood, A. E. and Major, A.: High-pressure reconnaissance investigations in the system Mg2SiO4-MgO-H2O, Earth Planet. Sci. Lett., 2, 130–133, https://doi.org/10.1016/0012-821X(67)90114-8, 1967.

Rigaku Oxford Diffraction: CrysAlisPro Software system, version 1.171.38.46, Rigaku Corporation, Oxford, https://rigaku.com/products/crystallography/x-ray-diffraction/application-notes/px018-crysalispro-software-package-single-crystal (last access: 14 September 2026), 2018.

Rothkirch, A., Gatta, G. D., Meyer, M., Merkel, S., Merlini, M., and Liermann, H. P.: Single-crystal diffraction at the Extreme Conditions beamline P02.2: Procedure for collecting and analyzing high-pressure single-crystal data, J. Synchrotron Radiat., 20, 711–720, https://doi.org/10.1107/S0909049513018621, 2013.

Wise, W. S. and Gill, R. H.: Minerals of the Benitoite Gem mine, Mineral. Rec., 8, 442–452, 1977.

Woodland, A. B., Girnis, A. V., Bulatov, V. K., Brey, G. P., and Höfer, H. E.: Breyite inclusions in diamond: experimental evidence for possible dual origin, Eur. J. Mineral., 32, 171–185, https://doi.org/10.5194/ejm-32-171-2020, 2020.

Yang, H. and Prewitt, T. C.: Crystal structure and compressibility of a two-layer polytype of pseudowollastonite (CaSiO3), Am. Mineral., 84, 1902–1905, https://doi.org/10.2138/am-1999-11-1224, 1999.

Zachariassen, W. H.: The crystal structure of benitoite, $BaTiSi_3O_9$, Z. Kristallogr., 74, 139–146, https://doi.org/10.1524/zkri.1930.74.1.139, 1930.